



ELSEVIER

Artificial Intelligence in Medicine 22 (2001) 193–214

**Artificial  
Intelligence  
in Medicine**

[www.elsevier.com/locate/artmed](http://www.elsevier.com/locate/artmed)

## A new virtual reality approach for planning of cardiac interventions

Thomas Sangild Sørensen<sup>a,b,\*</sup>, Søren Vorre Therkildsen<sup>a</sup>,  
Piotr Makowski<sup>c,1</sup>, Jørgen Lindskov Knudsen<sup>a</sup>,  
Erik Morre Pedersen<sup>b,2</sup>

<sup>a</sup>Computer Science Department, University of Aarhus Åbogade 34, 8200 Århus N, Denmark

<sup>b</sup>MR Research Centre, Institute of Experimental Clinical Research, Department of Cardiothoracic and Vascular Surgery, Aarhus University Hospital, Skejby Sygehus Brendstrupgårdsvej, 8200 Århus N, Denmark

<sup>c</sup>MR Research Centre, Institute of Electronics, Technical University of Lodz,  
Stefanowskiego 18/22, 90-537 Lodz, Poland

Received 22 March 2000; received in revised form 13 November 2000; accepted 11 December 2000

---

### Abstract

A novel approach to three-dimensional (3D) visualization of high quality, respiratory compensated cardiac magnetic resonance (MR) data is presented with the purpose of assisting the cardiovascular surgeon and the invasive cardiologist in the pre-operative planning. Developments included: (1) optimization of 3D, MR scan protocols; (2) dedicated segmentation software; (3) optimization of model generation algorithms; (4) interactive, virtual reality visualization.

The approach is based on a tool for interactive, real-time visualization of 3D cardiac MR datasets in the form of 3D heart models displayed on virtual reality equipment. This allows the cardiac surgeon and the cardiologist to examine the model as if they were actually holding it in their hands. To secure relevant examination of all details related to cardiac morphology, the model can be re-scaled and the viewpoint can be set to any point inside the heart. Finally, the original, raw MR images can be examined on line as textures in cut-planes through the heart models. © 2001 Elsevier Science B.V. All rights reserved.

*Keywords:* Pre-operative planning; Heart modeling; Virtual reality visualization

---

\* Corresponding author. Tel.: +45-89423-188; fax: +45-89425-624.

*E-mail addresses:* sangild@daimi.au.dk (T.S. Sørensen), svorre@daimi.au.dk (S.V. Therkildsen), makowski@ck-sg.p.lodz.pl (P. Makowski), jlk@daimi.au.dk (J.L. Knudsen), erik.morre@iekf.au.dk (E.M. Pedersen).

<sup>1</sup> Tel.: +48-426312642; fax: +48-426362238.

<sup>2</sup> Tel.: +45-89495-484; fax: +45-89496-016.

0933-3657/01/\$ – see front matter © 2001 Elsevier Science B.V. All rights reserved.

PII: S 0933-3657(00)00109-3

## 1. Introduction

When planning cardiac surgery or other cardiac interventions, pre-operative decisions are currently based on 2D image data and the ability of the surgeon or the cardiologist to translate these 2D images into a 3D understanding of the cardiac morphology. Especially in the case of complex congenital heart diseases where operation planning is crucial for an optimal result, a better pre-operative 3D understanding could minimize surgical explorations and have decisive importance for the detailed planning of the surgical procedure.

Virtual models have previously been used in different areas of surgery planning, e.g. dental, spine [8], and femur [26] surgery planning, as well as in virtual colonoscopy [35]. Virtual reality in neurosurgical planning has been examined [17] and augmented reality was used together with generic virtual cardiac models for teleconsultation in [4]. Documentation of previous approaches to 3D modeling of cardiac data in operative planning is sparse. Orthogonal planes have been used to visualize the data [32], holographic imaging have been used to print dynamic data [12], and the use of stereolithographic modeling has been used to obtain model hard copies [5]. In this paper, a novel approach to virtual reality visualization of cardiac data will be presented.

In the present study, we hypothesize that

- it is possible to generate morphologically accurate and detailed 3D surface models of the heart from high resolution MR image data;
- new intuitive, real-time ways of interacting with the 3D model has the potential to advance virtual reality visualization to a clinically useful tool for the planning of cardiac interventions;

The purpose of our work is then to

- establish a protocol for acquiring high resolution, high quality 3D cardiac imaging data suited for virtual reality visualization using state of the art magnetic resonance imaging (MRI) techniques;
- develop algorithms to generate morphologically reliable surface models of the heart based on MRI data;
- develop intuitive, real-time virtual reality visualization methods for the generated models;
- test the entire process on volunteers, interacting with medical doctors.

Four steps were involved in the process: (1) data acquisition; (2) segmentation; (3) model generation; and (4) virtual reality visualization (Fig. 1). Protocols and software were developed that each handled one task in the process.

### 1.1. Data acquisition

High resolution image data is needed to obtain detailed models. At the same time, image details and contrast features cannot be allowed to degrade at the expense of increasing resolution, since a high level of automatization is desired for segmentation of the images. Recent work with 3D echocardiography, e.g. [29,31], has shown that it provides sufficient

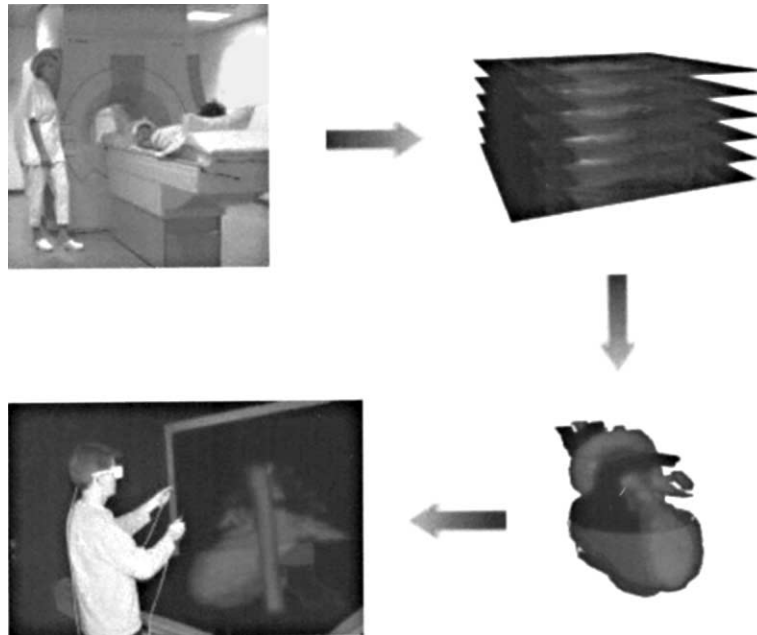


Fig. 1. The visualization pipeline. From scanning to virtual reality visualization. The involved steps are: (1) MR-scanning; (2) segmentation; (3) model generation; (4) visualization and interaction using hand held tracking devices.

resolution for generating a 3D model of the left ventricle for the purpose of determining its volume. For models of more subtle details though, the resolution and image quality is currently not sufficient. Recently, ECG triggered 3D cardiac helical computerized tomography has been introduced [24]. However, the contrast agents that must be used to achieve sufficient contrast between the soft tissues diffuse into the tissue resulting in a relatively poor contrast to noise ratio between the blood pool and the myocardium. MRI was early recognized as an accurate technique for describing cardiac dimensions [19]. Since then MRI has reached a level, where high resolution 3D images of the proximal coronary tree with sub-millimeter resolution can be obtained [6]. MRI is considered the golden standard for imaging of cardiac chamber volumes and myocardial masses.

### 1.2. Segmentation

The classification of pixels into regions, segmentation, is an area of active research. Methods which can claim to solve the segmentation problem for cardiac imaging have yet to be developed. For each pixel in an image it needs to be decided, whether the pixel is outside the heart, if it represents the myocardium, or the blood pool. Thresholding [27] is not applicable to cardiac MRI due to overlapping intensity intervals for the regions of interest. Edge detectors such as the Canny filter [7] and the Laplacian operator are sensitive to noise and their use in cardiac MRI would require thresholding of the resulting edge

images. This often leads to discontinuous regions, reducing the effectiveness of further processing. Region growing [1] and watersheds [37] are both methods to segment an image into closed regions. As the image contrast to noise in cardiac MRI improves, we believe that both methods will become applicable. Currently, we rely on active contour models, balloons [14] and snakes [10]. Dedicated software [21] for segmentation of 3D cardiac MR datasets was, thus, developed using a two-phase algorithm of: (1) a initial balloon approach; and (2) a snake approach that would then fine-tune the generated balloon to the exact positions of the desired edges. Examples of balloons extended to 3D for cardiac segmentation can be found in [9,23], though they only applied the 3D deformable models to segment the left ventricle, but no other cardiac geometries.

### *1.3. Model generation*

Several techniques to construct virtual models from medical images exist. A classical approach is the marching cubes algorithm [20], which uses thresholding on the raw volume data to generate an iso-surface. For large image volumes (as we are considering), this method creates too many polygons for smooth interactive visualization and locally even flawed surfaces. Many approaches exist to address these problems, e.g. [25,30]. Alternatively, the iso-surface construction can be based on distance fields [13]. Stitching together contours [2,15] is a different surface modeling technique. The approach taken in this paper is a slightly adapted implementation of the work presented in [2]. We also looked at volume rendering [11] for model generation and visualization. This is a promising approach as volume rendering hardware constantly improves in speed, but currently we find the delivered frame rates dissatisfactory for real-time visualization of large volumes. An overview of the most common data presentation techniques in pediatric cardiology was presented in [36].

### *1.4. Visualization*

A visualization set-up has traditionally consisted of a monitor and a 2D input device such as the mouse. Moving away from this basic set-up, virtual reality simulations are expected to be used by medical professionals at many levels in the future [28]. Display systems, which bring virtual models within physical reach of the user, in combination with 3D interaction devices are likely to become the platform of tomorrow. An example of a virtual reality interaction interface is given in [18]. In this paper, we show and discuss how the interpretation of a complex cardiac dataset benefits from moving to a true 3D visualization platform.

## **2. Material, methods, and technology**

### *2.1. Data acquisition*

High resolution 3D datasets covering the entire heart and large vessels from above the aortic arch to below the apex of the left ventricle were obtained on a Phillips 1.5T NT

scanner using a five-element cardiac synergy coil and CPR6 cardiac patch software. ECG triggering was applied to gate acquisitions to a 100 ms diastolic time window for suppression of cardiac motion. Respiratory compensation was obtained by using a real-time navigator technique with prospective slice correction. The navigator was placed on the diaphragm using a 4 mm acceptance window. The pulse sequence used was a 3D, T2-prepared segmented k-space gradient echo technique as recently developed for coronary artery imaging [6]. A  $256 \times 256$  matrix (reconstructed to  $512 \text{ mm} \times 512 \text{ mm}$ ) and a  $256 \text{ mm} \times 256 \text{ mm}$  field of view gave an in-plane resolution of  $1 \text{ mm} \times 1 \text{ mm}$ . A total of 60–75, 2 mm thick contiguous transversal slices were obtained in a total scan time of approximately 20–25 min during free breathing. The exact scan time depended on the respiration pattern and the heart rate.

## 2.2. Segmentation

Dedicated software [21] was developed to implement the proposed two-phase segmentation method.

### 2.2.1. Segmentation with balloons

Consider a discrete curve  $v$  with  $n$  vertices. Let  $v_l \in R^2$ ,  $l < n$  denote the coordinates of vertex  $l$ . Based on the edges connecting  $v_l$  to its neighboring vertices, the normal,  $\mathbf{n}_l$ , can be calculated. A balloon force vector for vertex  $v_l$  is set to  $s_l \mathbf{n}_l$ , where  $s_l$  is a scalar that determines the magnitude of movement parallel to the vertex normal. In an iterative process, both  $s_l$  and  $v_l$  are recalculated for each iteration. Since no other forces are used,  $s_l$  needs to be positive when the vertex is far from the desired point and it should decrease to zero as the point is approached. These demands are fulfilled setting  $s_l$  to the discrete version of  $S_l$  found as

$$S_l = p_1(\nabla I(x, y) \cdot \mathbf{n}_l) + p_2 I(x, y) + p_3 \left| \frac{d^2 v}{ds^2} \right| + p_4 \left| \frac{d^4 v}{ds^4} \right| \quad (1)$$

where  $I(x, y)$  is the image intensity in pixel  $(x, y)$  and  $p_k$  ( $k \in \{1, 2, 3, 4\}$ ) is a constant. When the vertex normal and the image gradient (edge normal) are parallel, the first term gives maximal contribution. When the vertex is far from an edge or when the vertex normal and the image gradient are not aligned, the term is close to zero. The second term makes the balloon inflate itself when it is within an area of high intensity. Since blood has high intensity and muscle low intensity, the term tends to zero when a muscle is reached, while it will inflate the balloon when far from an edge. The last two terms in the equation denote the curve elasticity and stiffness. This is a contribution similar to the elasticity and stiffness terms of the classical snakes.

### 2.2.2. Segmentation with snakes

To fine-tune the curves to the edges, the balloons were regarded as initializations to the classical snakes [14]. The major problem with the snakes as they were originally introduced, was exactly the problem of proper initialization. Using the curves defined by the balloons was expected to solve this initialization problem.

### 2.3. Model generation

The segmentation task resulted in a set of contours in parallel planes, defining different anatomical parts of the cardiovascular system. A 3D model was created by connecting these contours. The algorithm used to do this was derived from [2] with implementation details given in [34]. The algorithm consisted of two phases. In the first phase, it searched neighboring slices for parts of contours similar in shape and position. A voting procedure was used to determine this. The matching contour parts were then connected by a triangulation. Having triangulated all matches, clefts were left in areas with a high degree of change between slices, e.g. when a blood vessel splits from one slice to the next. The edges forming the cleft would be a 3D polygon.

**Definition.** A minimal weight triangulation (MWT) of a polygon is the triangulation with the shortest total edge length.

**Definition.** A *simple* polygon is a polygon that does not intersect itself and has no internal holes.

A MWT was found using an algorithm described in [16]. The algorithm used a dynamic programming approach to find the triangulation with the lowest sum of edge lengths. It worked, however, only on simple, 2D polygons. To obtain a 2D polygon, the 3D cleft was projected onto the  $xy$ -plane. If the 2D polygon was self-intersecting, it was split into two polygons. Each of these would be triangulated as a cleft. Clefts with internal holes can be transformed into simple polygons as described in [2].

### 2.4. Visualization in a virtual reality environment

#### 2.4.1. Hardware

Special virtual reality hardware used in this project included a Holobench, shutter glasses, tracking devices, and an Onyx2 (Figs. 1 and 4).

**2.4.1.1. Holobench.** The Holobench (Tan, Germany) set-up consisted of two displays, each measuring 180 cm  $\times$  110 cm and angled 90° at each other. One was standing vertically, the other horizontally, as placed in an 'L'.

**2.4.1.2. Shutter glasses.** In order to obtain the illusion of having objects lying in the workspace in front of the user, separate images reflecting different points of views were generated for each eye. To insure that each eye would see the correct image only, shutter glasses (Crystal Eyes, StereoGraphics, California, USA) were used.

**2.4.1.3. Tracking.** To register user movement, a head sensor, two styluses, and a Polhemus Fastrak (Polhemus, Vermont, USA) was used. The head sensor was used for tracking the users head position and orientation by attaching it to the glasses, in order to show the world as seen from the users point of view. The user was then able to move his head around an object in the model rather than move the object itself, to get better orientation. Two

Polhemus styluses, pencil-shaped tracking devices with buttons, were used for interaction with the model by gestures.

*2.4.1.4. Graphics station.* An Onyx2 InfiniteReality2 Rack (sgi, California, USA) with  $6\text{ MHz} \times 250\text{ MHz}$  MIPS R10000 processors and 1.5 Gb RAM. Two graphics pipelines were used to generate the real-time graphics.

#### *2.4.2. Interaction*

A scene interaction library [22] (RoninWorks, Maarssen, The Netherlands) based on input from two tracking devices was used for interaction. Running the application, the user placed his tracking devices (in our case the styluses) in space, where he wanted to grab the world. A marker (a jack) was introduced in the model to indicate the position of the styluses (Fig. 4). The user was then able to move (translate) the model while pressing a stylus button. This functionality applied to both styluses. By grabbing the world with both styluses simultaneously while pressing both buttons, the model could be zoomed and rotated by gestures. Zooming in was obtained by moving the hands apart, zooming out by moving the hands together. Rotation was performed by moving the hands in a rotational fashion, displacing them relative to each other. The two points marked by the styluses at the beginning of the manipulation would be transformed to the new positions marked by the styluses at the end of the manipulation.

#### *2.4.3. Clip planes for model validation*

An option to insert clip planes in the model was implemented to give the user a possibility to “open up” the model and take a look inside. Clip planes could be inserted and moved freely in real-time with either hand by using a stylus as a normal vector for positioning and orienting the plane.

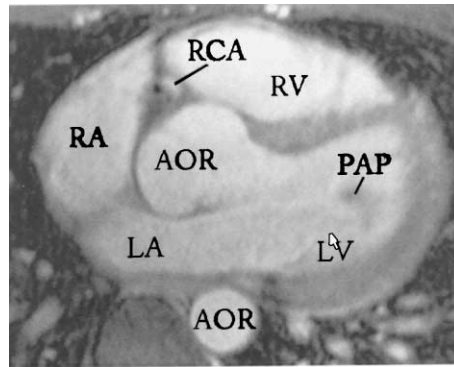
#### *2.4.4. Texture mapping for model validation*

A simple and fast form of volume visualization was implemented for model validation purposes, showing one, opaque image slice at a time for each hand. The clip plane described above defined the image slice plane. The two planes were displaced slightly, causing the model to peek through the textured plane, making it possible to compare the generated model to the raw data volume.

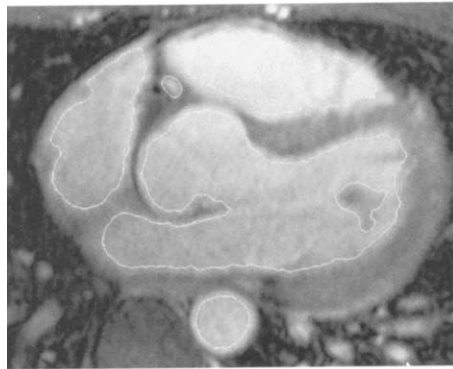
### **3. Results**

#### *3.1. Imaging and segmentation*

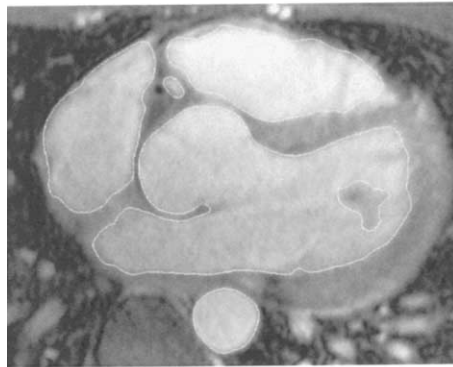
Fig. 2(a) shows a sample MR image from a transversal plane through the heart of a volunteer. The inner cardiac cavities, i.e. the ventricles, the atria, and the aortic root are well defined. Likewise, the descending aorta but also much smaller structures such as the coronary arteries, papillary muscles, and branches of the pulmonary vessels can be distinguished. A segmentation of the image, using only balloons and balloons followed



(a)



(b)



(c)

Fig. 2. Quality of imaging and segmentation. (a) Reference image from the scanner showing the right and left ventricles (RV, LV), right and left atria (RA, LA), the aortic root and descending aorta (AOR), a papillary muscle (PAP), the right coronary artery (RCA), and branches of the pulmonary vein in the lower right corner. (b) Segmentation using balloons only. The 'island' within the left ventricle is a papillary muscle. (c) Segmentation using balloons followed by snakes.

by snakes, respectively, is seen in Fig. 2(b) and (c). Fig. 2(b) illustrates how the balloons are often not inflated all the way to the edges. In Fig. 2(c), the effect of using snakes to fine-tune the contours right to the edges between the myocardium and the blood pool is seen. The contours were color-coded to provide guidance to which contours should be connected during the model generation step.

### 3.2. Model generation

The parts of the contours that were matched in the first phase of the model generation program, provided smooth surfaces. An example of the second phase, the MWT, is shown in Fig. 3(a). Unfortunately, as the figure shows, the MWT algorithm often created small ledges in the triangulation. To avoid this, the weight function of the MWT was modified to punish with extra weight, triangles having all vertices in the same contour. This changed the behavior of the cleft triangulation, to use as many triangles as possible to connect points in the two contours, reducing the number of ledges. The modification of the weight function created a smoother looking triangulation, as seen in Fig. 3(b).

The number of polygons in the model created using contour matching on a volume of  $512 \times 512 \times 75$  voxels with different point spacing can be seen in Table 1. Using any of the point distances resulted in smooth surfaces. In comparison to an often used algorithm ‘Marching Cubes’ [20] on the raw data, the polygon count of the contour matching model is substantially lower. The original marching cubes algorithm would generate a surface of nearly 670,000 polygons on the same volume. The contour matching algorithm runs fully automatically and is fast (less than 2 min).

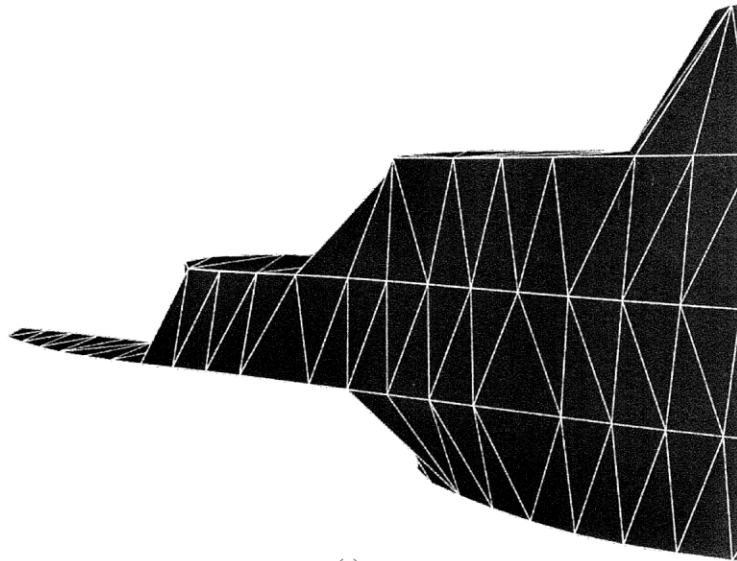
### 3.3. Virtual reality visualization

The developed virtual reality scenario is illustrated in Fig. 4. The generated 3D models were studied at the Holobench using real-time interaction to freely rotate, scale and move the heart and to insert clip planes and raw image data in any plane. The interaction was performed by simply moving the hands when holding and activating the stylus trackers. Two jacks (white arrows) visualized the hand movements in the 3D world.

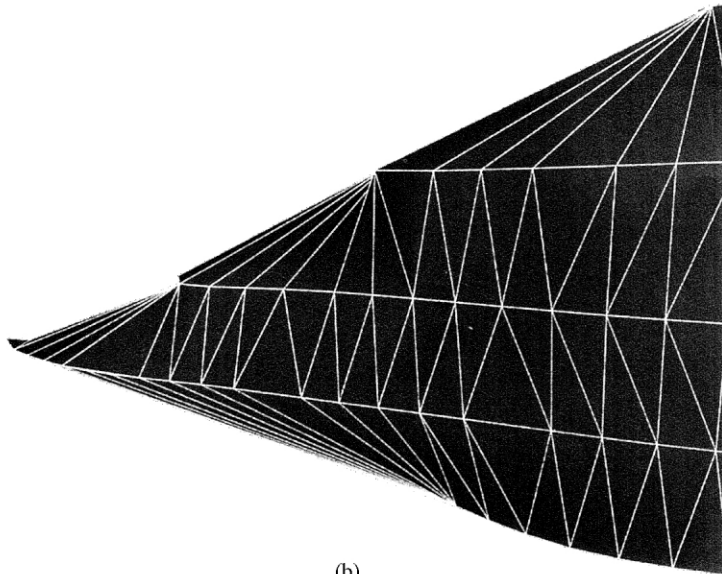
### 3.4. Case study: visualization of a normal heart in virtual reality

Data from a study of a normal volunteer is shown below. In Fig. 5(a), the generated 3D model of the heart is seen from behind. All the structures on the posterior side of the heart including pulmonary veins, pulmonary arteries and coronary sinus were visualized and their anatomic relations could be studied. When looking inside the aorta (Fig. 5(b)), the detailed configuration and size of the ostia of the vessels branching off the aortic arch are seen.

In Fig. 6(a), the same heart model has now been rotated and is seen from the right. The structure of the caval veins leading blood back to the heart into the right atrium is clearly seen. Also the right coronary artery and its relation to the right ventricle and atrium can be seen. In this example, the myocardium is overlaid as a partly transparent layer allowing estimates of the thickness of the cardiac muscle. In a view from the inside of the right



(a)



(b)

Fig. 3. A vessel, which is only visible in a few slices. (a) Surface resulting from the minimum weight triangulation. (b) Surface resulting from the modified weight triangulation that punishes triangles with all vertices in one contour.

Table 1  
The number of polygons generated by contour matching a  $512 \times 512 \times 75$  voxel volume

Point spacing along contour (pixel)	Polygons in model
1	164128
2	82237
3	54936
4	41296

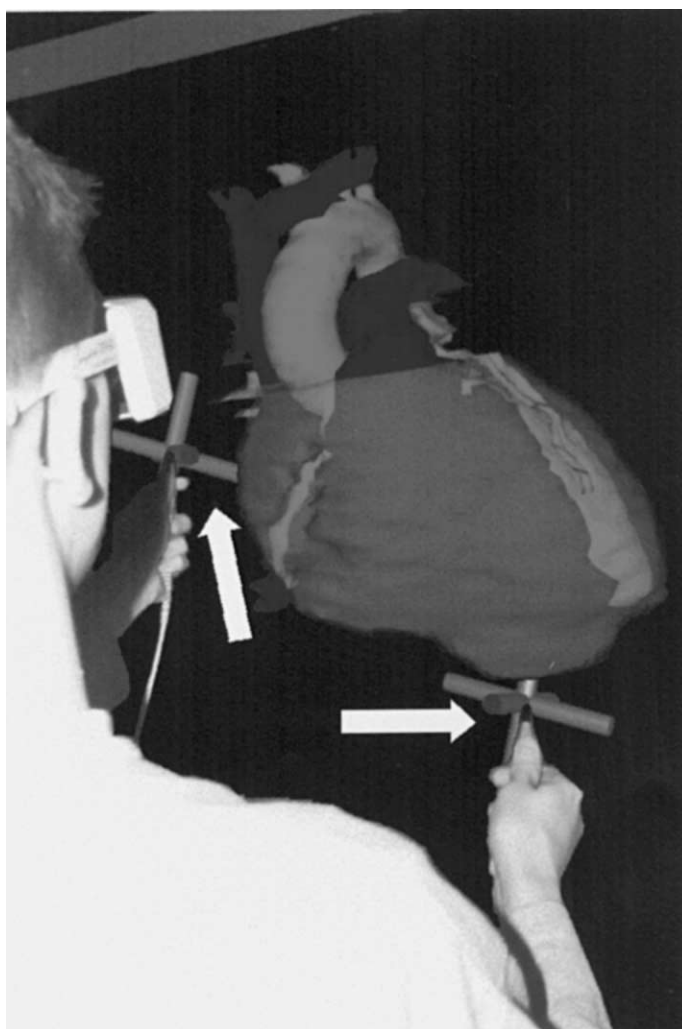


Fig. 4. Visualization of the generated model in an interactive, real-time virtual reality set-up. Shutter glasses are used to make the model appear in the space spanned by the two screens in front of the user. The tracked styluses are used for interaction with the models based on gestures. The styluses control the jacks (indicated by the white arrow), which represent the position of the users hands in the virtual space.

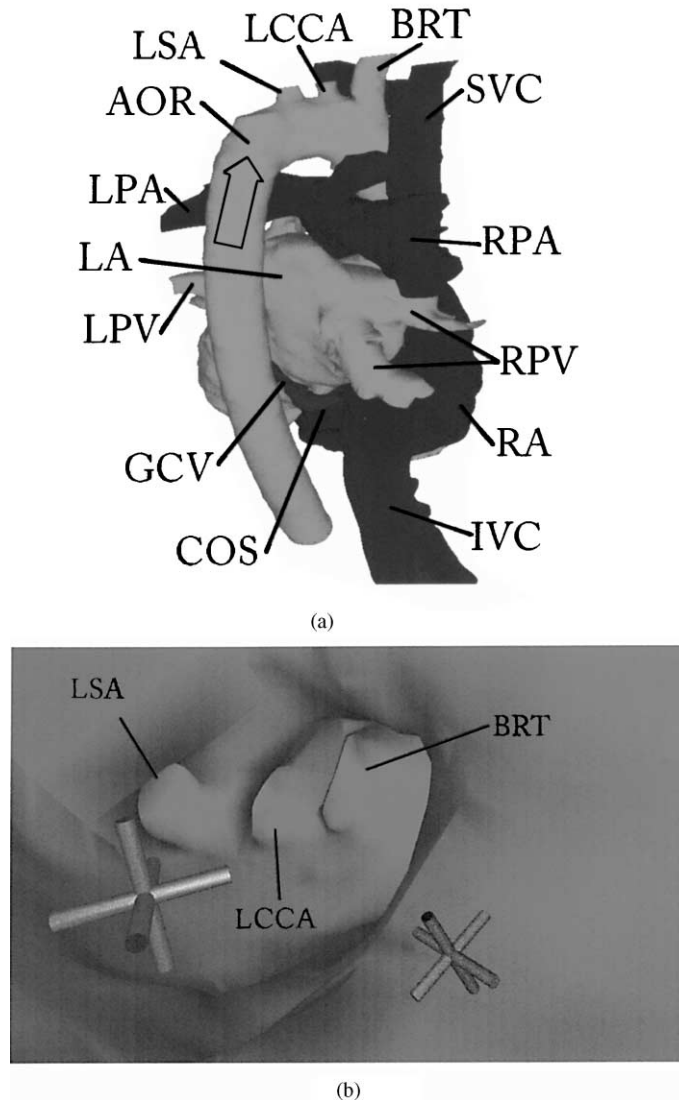
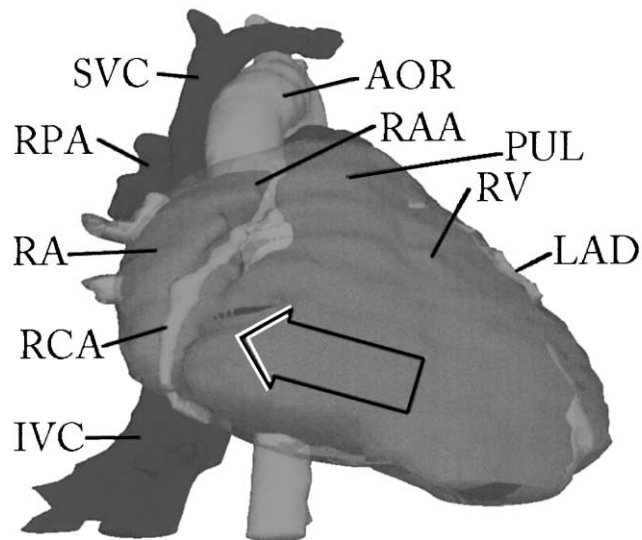
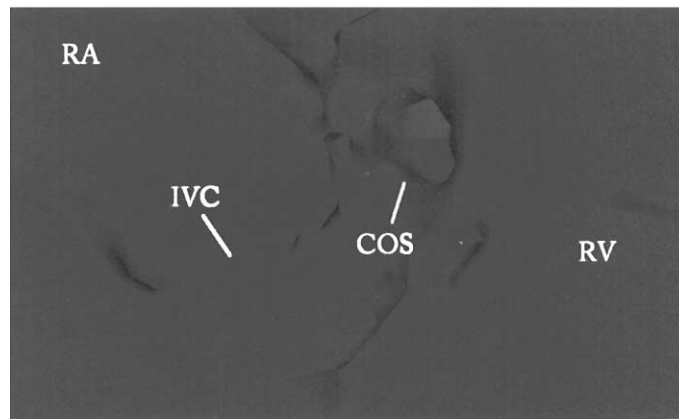


Fig. 5. Aortic arch visualization. A 3D model from a normal volunteer is seen from behind. (a) The aorta (AOR) with the brachiocephalic trunk (BRT), left common carotid artery (LCCA), and left subclavian artery (LSA) are clearly visualized together with the main structures on the posterior side of the heart, right pulmonary artery (RPA), left pulmonary artery (LPA), left pulmonary veins (LPV), right pulmonary veins (RPV), and the great cardiac vein (GCV) entering the coronary sinus (COS) as well as the superior (SVC) and inferior (IVC) caval veins. (b) The aortic arch is viewed from the inside in the direction given by the arrow in (a). The BRT, LCCA and LSA ostia are seen in detail.



(a)

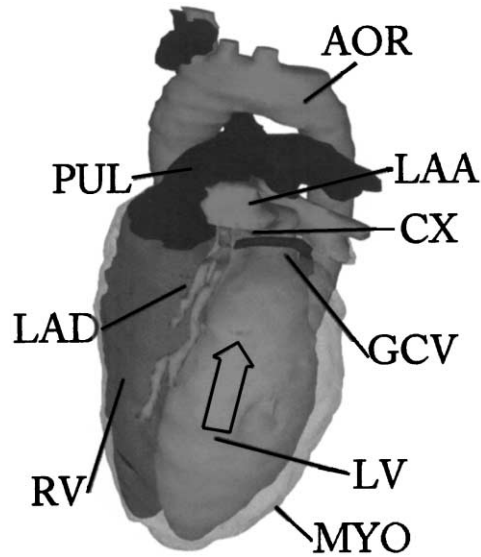


(b)

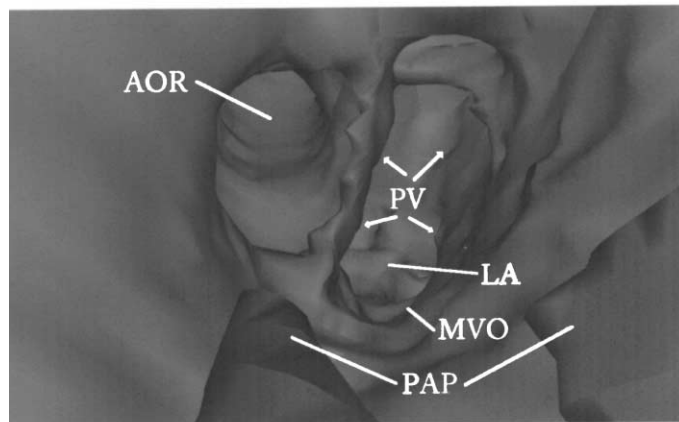
Fig. 6. Right heart visualization. The same 3D model as in Fig. 5 is now seen from the right side. (a) The right coronary artery (RCA) can be followed from the aorta and along the groove between the right atrium (RA) and the right ventricle (RV). The aorta (AOR), left anterior descending coronary artery (LAD), superior (SVC) and inferior (IVC) caval veins are also seen. The myocardium (MYO) is overlaid as a partly transparent layer. (b) The right atrium is seen as viewed from the inside at the level of the tricuspid valve in the direction given by the arrow in (a). The coronary sinus (COS) is clearly seen entering the atrium.

atrium (Fig. 6(b)), the entrance of the coronary sinus into the atrium and its relation to atrial structures can be studied.

Looking at the model from the left side (Fig. 7(a)), details of the left coronary artery system and its anatomic relations can be studied. The proximal part of the circumflex and



(a)



(b)

Fig. 7. Left heart visualization. The 3D model seen from the left side. (a) The relations between the left anterior descending coronary artery (LAD) with diagonal branches, the great cardiac vein (GCV) and the circumflex coronary artery (CX) can be seen. Also the aorta (AOR), pulmonary trunk (PUL) and left ventricle (LV) can be seen. The lower part of the left atrial appendage (LAA) has been removed to be able to see the most proximal part of the left coronary arteries. (b) The left ventricle is seen from the inside in the direction given by the arrow in (a), looking into the oval mitral valve orifice (MVO) and the more circular aortic orifice. The branching of the pulmonary veins (PV) in the left atrium (LA) can be seen as well as papillary muscles (PAP).

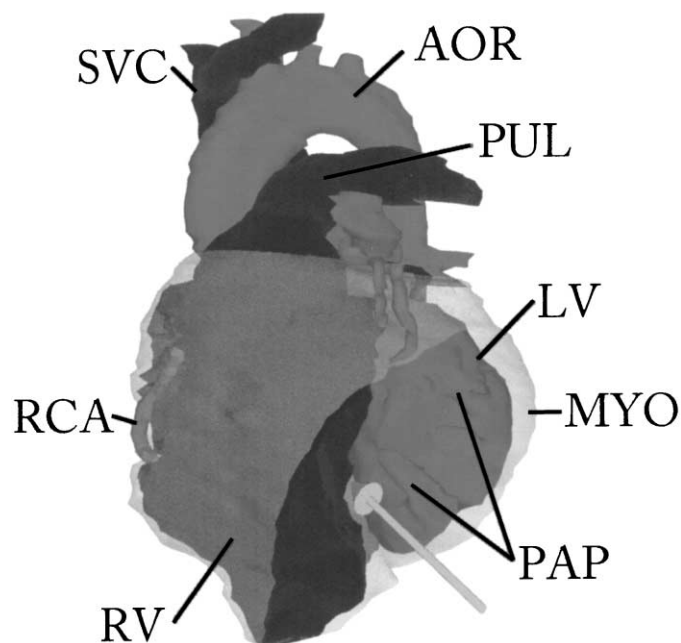


Fig. 8. Adding clip planes to the model. The clip plane is perpendicular to the arrow. Details like, e.g. myocardial thickness (MYO) and exact distances between structures in the plane can be studied. In this example, the plane is cutting through the left ventricle (LV) and the papillary muscles (PAP). The pulmonary trunk (PUL), aorta (AOR), right atrium (RA), right ventricle (RV), right coronary artery (RCA), and superior vena cava (SVC) can also be seen.

left anterior descending coronary artery and its first diagonal branches are visualized together with the great cardiac vein. Looking inside the left ventricle from the apex (Fig. 7(b)), the mitral and aortic valve openings can be seen, and details like pulmonary vein inlets in the left atrium and also papillary muscles can be studied.

The clip plane feature is demonstrated in Fig. 8. By activating a button, the stylus tracker is turned into a clip plane tool that places a plane in the model and cuts away the part of the model between the user and the clip plane. This is performed in real-time, and the clip plane can be freely chosen. Its position is visualized in the form of an arrow perpendicular to the plane (Fig. 8). The same technique is used for defining clip planes on which the original image data is pasted in order to be able to validate the reliability of the generated model (Fig. 9). As for the basic clip plane, a plane can be freely chosen by each hand with the results displayed in real-time.

#### 4. Discussion

A real-time, Holobench-based system was developed for interactive 3D visualization of the heart and great vessels. To our knowledge, it is the first time that such a system has been

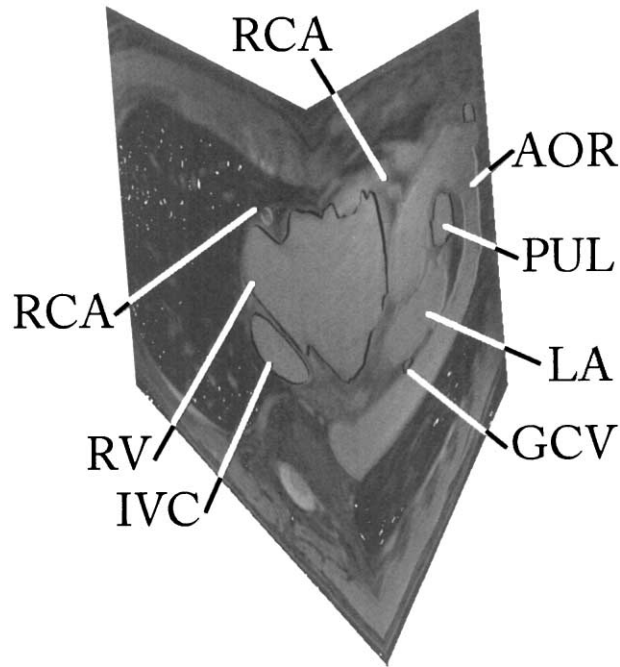


Fig. 9. Application of the clip plane tool with original image data pasted onto the clip plane. The model peeks through the image data for validation purposes. Two clip planes are inserted at different angles showing the right coronary artery (RCA), left atrium (LA), great cardiac vein (GCV), inferior vena cava (IVC), left atrium (LA), pulmonary trunk (PUL) and the aorta (AOR).

presented for intended use in pre-operative planning of cardiac interventions. The features to be implemented were determined through sessions with cardiac surgeons and cardiologists.

#### 4.1. Hypothesis, revisited

The first hypothesis of the study was approved in as much as morphologically accurate and detailed 3D surface models of the heart could be generated from high quality, high resolution, non-contrast-based, free breathing 3D prospective navigator corrected MR cardiac images.

The second hypothesis of advancing virtual reality to potential clinical usefulness in cardiac intervention planning is harder to test. However, we think that we have demonstrated an approach that contains this potential. Visualizing high quality surface models in virtual reality with interaction based on gestures in real-time, provided a very high degree of 3D understanding. In addition to the stereo vision, the movement of the hands in space added 3D experience associable to the way the heart is operated on during surgery. Finally, the successful application in volunteers where detailed models could be generated, adds to

the feasibility of the overall approach. Clinical studies are in progress to explore this hypothesis further. We believe that the possibility to freely interchange between the virtual model and the raw image data will eventually allow for making ‘on line’ definitive decisions, as image artifacts and possible artifacts related to the model generation can be resolved immediately.

#### 4.2. *Imaging and segmentation*

New real-time, navigator-based 3D, MRI techniques provided the basis for obtaining slices with sufficient signal to noise with minimal artifacts from respiratory movement, that would otherwise have caused considerable motion artifacts and image blurring. The scan time needs to be reduced to less than the current 20–25 min, before being routinely applicable in patients. The gradient echo technique used for image acquisition was not ideal as it generated image contrast depending on the velocities of blood that varied throughout the cardiac chambers. Despite the ability of the T2-preparation to create a high contrast to noise between myocardium and the blood pool [6], the varying velocities limited the potential for a fully automatic segmentation.

At present, the developed segmentation application [21] is semi-automatic, and it provides us with a tool to segment and validate an image volume in a reasonable amount of time (approximately 5 h). This is acceptable when considering, e.g. pre-operative surgery planning of complex congenital heart diseases, but not for more routine clinical problems. We estimate that the segmentation tool speeds up the segmentation with a factor of five compared to fully manual segmentation. Continued effort will be put into improving both the image contrast to noise and the segmentation tool to shorten the segmentation time. The time consuming part of the segmentation process is manually editing contours, which do not represent the desired edges satisfactorily. Hence, we supplemented our segmentation software with efficient tools to manually edit contours in images the algorithm could not handle properly.

We are aware that extending the balloons to 3D would have combined segmentation and model generation to one task. However, this would be significantly more complicated computationally. Furthermore, it was important to be able to validate and possibly manually correct the segmentation of a dataset. This would be done by presenting the cardiologists with the 2D images they are used to work with, and then examine the segmentation in each image. Finally, methods exist to fully automatically create 3D surfaces from 2D contours, which allowed us to focus on the ‘simpler’ 2D segmentation compared to its 3D alternatives.

It should be emphasized that the segmentation is not a part of the diagnostic process. It is a practical tool to extract the relevant data. It should be approved by an imaging professional before model generation is performed and the resulting model is presented to the surgeon or the invasive cardiologist.

Preliminary results from image experiments in pigs using the new blood pool agent NC100150 Injection BPCA (Nycomed Imaging A/S, Sweden) has indicated, that images suitable for highly automated segmentation can be obtained in the future, as also proposed in [33].

### 4.3. Model generation

A model created by the described algorithm reflected the segmentation closely, leaving it to a matter of a valid segmentation to obtain a morphologically correct model. Since the segmentation can be validated by experts, the model was reliable. Also, the precision of the model was verified interactively with the textured clip planes. This was a decisive property, since it provided the user, who had not necessarily been involved in the segmentation process, with a fast and efficient tool to examine the accuracy of the model.

The approach handled splitting vessels and other changes between slices well. The split into first triangulating matching contour parts and then triangulating clefts, made it possible to create complicated surface structures, as was documented in the case study above. The simple triangulation of matching contours was intuitively reasonable when dealing with two equally sized sequences of points, which by definition were similar in shape and of equal arc length. When triangulating a cleft, it would be possible in some cases to create a valid triangulation directly from the 3D cleft itself, instead of projecting it into a plane before triangulation. It is, however, not always possible to triangulate a 3D polygon without obtaining self intersecting polygons. To determine whether a 3D polygon can be triangulated legally is a NP-complete problem [3]. Triangulating a simple, 2D polygon is straight forward though as described previously, making it a feasible approach.

The contours were represented as Hermite splines with the vertices defining control points. This allowed us to re-sample the contours at any resolution to control the polygon count. This made the models well suited for visualization in an interactive, real-time environment. A suspected improvement in image resolution in the future, will have the effect of generating smoother models. Since the polygon count in the models are easily controllable, this is not expected to have a degrading effect on the real-time performance of the system.

### 4.4. Virtual reality visualization

The virtual reality set-up imitated a natural working environment for many clinical tasks. The surgeon, who performs operations in a standing position daily, was comfortable standing at the Holobench with a stylus in each hand. Hereby, the virtual world was linked closely to the real world. Future improvements would be development of navigation tools, that directly simulate the hand movements and the tools used for cardiac surgery and for catheter-based interventions.

If the user placed himself centered to the screens, their sizes would cause his entire field of vision to be covered by the displays no matter whether he looked forwards or down. The effect was that he would get a sense of a workspace in front of him, where he could manipulate objects without having the illusion broken due to off-screen disturbance in his visual field. Using stereo vision as described previously, the user would get a sensation of objects actually being situated in the space spanned by the two screens. He could manipulate these objects by reaching into the workspace where the objects seemed to be located and do manipulations here, without having the screen as an obstacle. Any object could be enlarged and entered, giving the user the illusion of being inside the object. The

interface was generally mentioned as intuitive and easy to use after a short tutorial. After 15 min most users were able to move around in the model and they had learned to rotate and re-scale it repeatedly to maintain a good overview.

Occasionally, it was experienced that the users lost their sense of orientation, when inside some complex geometrical part of the anatomy, that had been scaled up and rotated extensively. To prevent this, we introduced a compass to indicate the primary axis in the lower-left part of the Holobench. The compass was drawn on top of all other geometry, making it visible at all times. Unfortunately, it proved to be an insufficient help to resolve the disorientation problems that occurred under the specific conditions. A solution could be to replace the compass with a miniature cardiac model, to provide both position and orientation in the model at all times.

Currently, the textures in the validation tool often hide the polygon model (Fig. 9). At one stage in the development phase, we implemented a version where only voxels classified as blood would show as opaque textures, the rest being fully transparent. The model would then always be visible. However, the cardiologist and the surgeon wanted to use the tool partly to see, if the model was missing any features in the dataset. For this reason, we decided to show the entire texture. Future work should try to combine the two approaches.

#### 4.5. Perspectives

MRI is currently the most promising technique to obtain the necessary signal to noise, soft tissue contrast, image resolution, and movement compensation for cardiac imaging. Dedicated cardiovascular MR scanners are now being developed and introduced into the market. This is expected to lead to continued improvements in scan time reduction, coil technology, and pulse sequences over the coming years and to finally allow dynamic, isotropic 3D datasets to be obtained with sufficient resolution and contrast features. Specifically, new intravascular contrast agents currently under approval for human use, has the potential to create a much higher contrast to noise between the myocardium and the blood pool of the inner cavities, while maintaining or even improving resolution [33]. Potentially this could result in a highly automatic segmentation, hereby reducing the time and effort currently limiting the effectiveness of the entire pipeline.

Computer hardware has reduced rapidly in price in recent years, giving reasonable priced personal computers that provide high graphical performance. Already at present, ordinary desktop monitors exist, that can display stereo graphics. In the near future, the visualization application will be ported to such platforms, to evaluate its performance on equipment that can be installed at hospitals at a low cost. Also in the near future, the different tasks presented in the imaging pipeline will be integrated in a common environment.

In addition to surgery and catheter-based intervention planning of congenital cardiac diseases, the developed virtual reality technology holds potential for other applications in the cardiac arena, such as adult cardiac surgery. If all steps, including image acquisition, segmentation, model generation, and visualization could be performed in a time and cost efficient manner in a routine clinical setting, other less complex cardiac problems in the adult population might also benefit from these visualization techniques. Also, similar

visualization approaches has been proposed for general medical use with focus on e.g. virtual bronchoscopy and virtual angiography [18].

## 5. Conclusion

A novel virtual reality approach to visualize morphologically accurate, 3D cardiac models based on MR data was developed. The techniques have potential to provide the surgeon and the interventional cardiologist with a real-time, interactive environment for pre-interventional planning and on line clinical decision-making based on the original imaging data. Ongoing improvements in imaging technology, interactive tools and display systems, continued with evaluation of the clinically added value, will determine the final role of these virtual reality techniques in the pre-operative planning of cardiac surgery and catheter-based interventions.

## Acknowledgements

The work has been carried out at the Centre for Advanced Visualization and Interaction (CAVI), sponsored by The Danish National Centre for IT Research (CIT) and the University of Aarhus. Also funding from the Karen Elise Jensen Foundation, and The Danish Heart Foundation grant 97-2-1-5-22549 and grant 00-1-3-68-22816.

## References

- [1] Adams R, Bischof L. Seeded region growing. *IEEE Trans Pattern Anal Mach Intell* 1994;16:641–7.
- [2] Barquet G, Sharir M. Piecewise-linear interpolation between polygonal slices. *Comp Vis Image Understanding* 1996;63:251–72.
- [3] Barquet G, Dickerson M, Eppstein D. On triangulating three-dimensional polygons. *Comput Geom: Theory Appl (CGTA)* 1998;10:155–70.
- [4] Berlage T. Augmented-reality communication for diagnostic tasks in cardiology. *IEEE Trans Information Technol Biomed* 1998;2:169–73.
- [5] Binder TM, Moertl D, Mundigler G, Rehak G, Franke M, Delle-Karth G, Mohl W, Baumgartner H, Maurer G. Stereolithographic biomodeling to create tangible hard copies of cardiac structures from echocardiographic data. *J Am College Cardiol* 1999;35:230–7.
- [6] Botnar RM, Stuber M, Danias PG, Kissinger KV, Manning WJ. Improved coronary artery definition with T2-weighted, free-breathing, three-dimensional coronary MRA. *Circulation* 1999;99:3139–48.
- [7] Canny J. A computational approach to edge detection. *IEEE Trans Pattern Anal Mach Intell* 1986;8:679–98.
- [8] Cleynebreugel JV, Verstecken K, Marchal G, Suetens P. A flexible environment for image guided virtual surgery planning. In: *Proceedings of the 4th International Conference on Visualization in Biomedical Computing*, Vol. 501, 1996. p. 510–24.
- [9] Cohen I, Cohen LD, Ayache N. Using deformable surfaces to segment 3D images and infer differential structures. *Computer Vision, Graphics, and Image Processing: Image Understanding* 1992;56:242–63.
- [10] Cohen LD. On active contour models and balloons. *Computer Vision, Graphics, and Image Processing: Image Understanding* 1991;53:211–8.
- [11] Eckel G. *OpenGL Volumizer Programmer's Guide*. Silicon Graphics, 1999.

- [12] Hunziker PR, Smith S, Scherrer-Crosbie M, Liel-Cohen N, Levine RA, Nesbitt R, Benton SA, Picard MH. Dynamic holographic imaging of the beating human heart. *Circulation* 1999;5:1–6.
- [13] Jones MW, Chen M. A new approach to the construction of surfaces from contour data. *Comp Graph Forum* 1994;13:75–84.
- [14] Withkin A, Terzopoulos D. Snakes: active contour models. *Int J Comp Vision* 1988;4:321–31.
- [15] Klein R, Schilling A, Strasser W. Reconstruction and simplification of surfaces from contours. In: *Proceedings of the Pacific Graphics'99, 1999*. p.198–207.
- [16] Klincsek GT. Minimal triangulations of polygonal domains. *Ann Discrete Math* 1980;9:121–3.
- [17] Kockro RA, Serra L, Tseng-Tsai Y, Chan C, Yih-Yian S, Gim-Guan C, Lee E, Hoe LY, Hern N, Nowinski WL. Planning and simulation of neurosurgery in a virtual reality environment. *Neurosurgery* 2000;46:118–37.
- [18] Krapichler C, Haubner M, Löscher A, Schuhmann D, Seemann M, Englmeier KH. Physicians in virtual environments-multi-modal human-computer interaction. *Interacting Comp* 1999;11:427–452.
- [19] Longmore DB, Klipstein RH, Underwood SR, Firmin DN, Hounsfield GN, Watanabe M, Bland C, Fox K, Poole-Wilson PA, Rees RS. et al. Dimensional accuracy of magnetic resonance in studies of the heart. *Lancet* 1985;1(8442):1360–2.
- [20] Lorensen W, Cline H. Marching cubes: a high resolution 3D surface construction algorithm. *ACM Comp Graph* 1987;21:163–70.
- [21] Makowski P, Sørensen TS, Therkildsen SV, Stødkilde-Jørgensen H, Pedersen EM. Two phase segmentation method for cardiac MRI data involving deformable contour and deformable model. In: *Proceedings of the 8th Scientific Meeting, International Society for Magnetic Resonance in Medicine, 2000*. p. 1547.
- [22] Mapes DP, Moshell MJ. A two-handed interface for object manipulation in virtual environments. *PRESENSE: Teleoperators Virtual Environ* 1995;4:403–16.
- [23] McInerney T, Terzopoulos D. A dynamic finite element surface model for segmentation and tracking in multidimensional medical images with application to cardiac 4D image analysis. *Comput Med Imaging Graph* 1995;19:69–83.
- [24] Mochizuki T, Murase K, Higashino H, Koyama Y, Doi M, Miyagawa M, Nakata S, Shimizu K, Ikezoe J. Two- and three-dimensional CT ventriculography: a new application of helical CT. *Am J Roentgenol* 2000;174:203–8.
- [25] Poston T, Nguyen HT, Heng PA, Wong TT. Skeleton climbing: fast iso-surfaces with fewer triangles. In: *Proceedings of the Pacific Graphics'97*.
- [26] Richolt JA, Teschner M, Everett P, Girod B, Millis MB, Kikinis R. Planning and evaluation of re-orienting osteotomies of the proximal femur in cases of SCFE using virtual three-dimensional models. In: *Proceedings of the 1st International Conference on Medical Image Computing and Computer-Assisted Intervention, 1998*. p. 1–8.
- [27] Sahoo PK, Soltani S, Wong AKC, Chen YC. A survey of thresholding techniques. *Comp Vision Graph Image Process* 1988;41:233–60.
- [28] Satava RM, Jones SB. Current and future applications of virtual reality for medicine. *Proc IEEE* 1998;86:484–9.
- [29] Schmidt MA, Ohazama CJ, Agyeman KO, Freidlin RZ, Jones M, Laurienzo JM, Brennehan CL, Arai AE, Ramm OT, Panza JA. Real-time three-dimensional echocardiography for measurement of left ventricular volumes. *Am J Cardiol* 1999;84:1434–9.
- [30] Shekhar R, Fayyad E, Yagel R, Cornhill JF. Octree-based decimation of marching cubes surfaces. In: *Proceedings of the Visualization'96, 1996*. p. 335–42.
- [31] Shiota T, McCarthy PM, White RD, Qin JX, Greenberg NL, Flamm SD, Wong J, Thomas JD. Initial clinical experience of real-time three-dimensional echocardiography in patients with ischemic and idiopathic dilated cardiomyopathy. *Am J Cardiol* 1999;84:1068–73.
- [32] Sklansky MS, Nelson TR, Pretorius DH. Usefulness of gated three-dimensional fetal echocardiography to reconstruct and display structures not visualized with two-dimensional imaging. *Am J Cardiol* 1997;80:665–8.
- [33] Stillman AE, Wilke N, Jerosch-Herold M. Use of an intravascular T1 contrast agent to improve MR cine myocardial-blood pool definition in man. *J Magnetic Resonance Imaging* 1997;7:765–7.

- [34] Therkildsen SV, Sørensen TS. Visualization of the cardiovascular system in a virtual reality environment for pre-operative planning of cardiac surgery. Master's thesis, Computer Science Department, University of Aarhus, 2000.
- [35] Valev V, Wang G, Vannier MW. Techniques of CT colonography (virtual colonoscopy). *Crit Rev Biomed Eng* 1999;27:1–25.
- [36] Vick III GW. Three- and four-dimensional visualization of magnetic resonance imaging datasets in pediatric cardiology. *Pediatric Cardiol* 2000;21:27–36.
- [37] Vincent L, Soille P. Watersheds in digital spaces: an efficient algorithm based on immersions simulations. *IEEE Trans Pattern Anal Mach Intell* 1991;13:583–98.